

---

# OPHIUCHUS: SCALABLE MODELING OF PROTEIN STRUCTURES THROUGH HIERARCHICAL COARSE-GRAINING $SO(3)$ -EQUIVARIANT AUTOENCODERS

**Allan dos Santos Costa**  
Center for Bits and Atoms  
MIT Media Lab, Molecular Machines  
allanc@mit.edu

**Ilan Mitnikov**  
Center for Bits and Atoms  
MIT Media Lab, Molecular Machines

**Mario Geiger**  
Atomic Architects  
MIT Research Laboratory of Electronics

**Manvitha Ponnampati**  
Center for Bits and Atoms  
MIT Media Lab, Molecular Machines

**Tess Smidt**  
Atomic Architects  
MIT Research Laboratory of Electronics

**Joseph Jacobson**  
Center for Bits and Atoms  
MIT Media Lab, Molecular Machines

## ABSTRACT

Three-dimensional native states of natural proteins display recurring and hierarchical patterns. Yet, traditional graph-based modeling of protein structures is often limited to operate within a single fine-grained resolution, and lacks hourglass neural architectures to learn those high-level building blocks. We narrow this gap by introducing Ophiuchus, an  $SO(3)$ -equivariant coarse-graining model that efficiently operates on all heavy atoms of standard protein residues, while respecting their relevant symmetries. Our model departs from current approaches that employ graph modeling, instead focusing on local convolutional coarsening to model sequence-motif interactions in log-linear length complexity. We train Ophiuchus on contiguous fragments of PDB monomers, investigating its reconstruction capabilities across different compression rates. We examine the learned latent space and demonstrate its prompt usage in conformational interpolation, comparing interpolated trajectories to structure snapshots from the PDBFlex dataset. Finally, we leverage denoising diffusion probabilistic models (DDPM) to efficiently sample readily-decodable latent embeddings of diverse miniproteins. Our experiments demonstrate Ophiuchus to be a scalable basis for efficient protein modeling and generation.

## 1 INTRODUCTION

Proteins form the basis of all biological processes and understanding them is critical to biological discovery, medical research and drug development. Fortunately, their three-dimensional structures often display modular organization across multiple scales, making them promising candidates for modeling in motif-based design spaces [Bystroff & Baker (1998); Mackenzie & Grigoryan (2017); Swanson et al. (2022)]. Harnessing these coarser, lower-frequency building blocks is of great relevance to the investigation of the mechanisms behind protein evolution, folding and dynamics [Mackenzie et al. (2016)], and may be instrumental in enabling more efficient computation on protein structural data through coarse and latent variable modeling [Kmieciak et al. (2016); Ramaswamy et al. (2021)].

Deep learning models have been shown to produce representations that capture high-level patterns of the data [Olah et al. (2018)]. Recent developments in learning architectures to protein structures

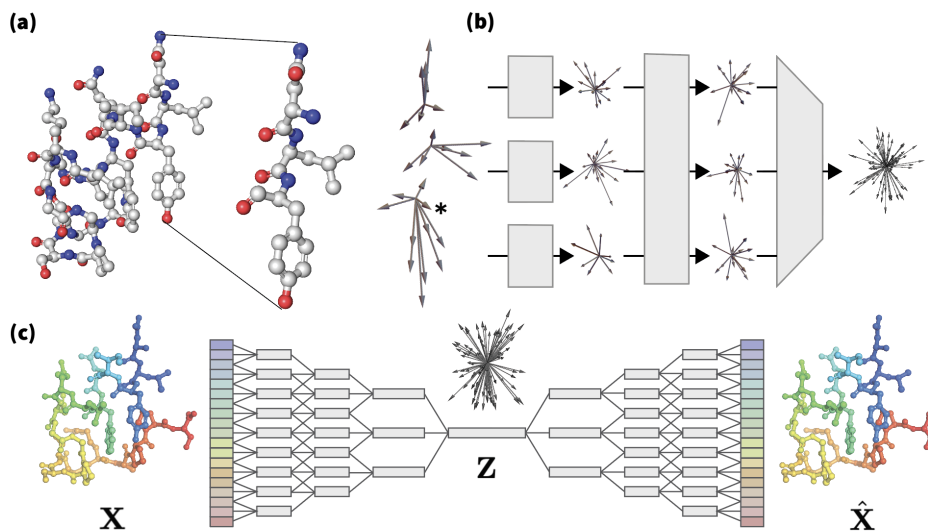


Figure 1: **Coarsening a Three-Dimensional Sequence:** (a) Ophiuchus takes atoms directly as representations of  $SO(3)$ . Non-scalar signals are taken relative to the  $C_{\alpha}$  position of the corresponding residue. Only 3D vector  $V^{l=1}$  components are shown. (\*) Unorderable atoms are encoded in a permutation invariant way. (b) Our proposed model uses three building blocks to transform those vectors and their anchors into coarser representations of coordinates. (c) We train a deep bottlenecking model by iteratively coarsening and refining across the sequence axis.

demonstrates the remarkable capabilities of neural models in the domain of protein modeling and design [Jumper et al. (2021); Baek et al. (2021b); Ingraham et al. (2022); Watson et al. (2022)]. Still, current state-of-the-art learning architectures often fail to incorporate inductive biases necessary for directly representing high-level components, such as coarsening of representations over the data domain.

To fill this gap, we introduce Ophiuchus, a deep convolutional model that captures joint encodings of sequence-structure motifs of all-atom protein structures. Our model contracts representations over the sequence to produce compressed encodings in hierarchical fashion. To capture three-dimensional geometry effectively, we model features as irreducible representations of  $SO(3)$ , introducing novel roto-translational equivariant neural architectures for multi-layer hourglass-shaped autoencoder.

We ablate the reconstruction performance of different network layouts and compression settings. We investigate the learned latent space and show it to produce rich representations that are directly employable in structural interpolation. Finally, we deploy a diffusion model on the latent space of Ophiuchus to investigate the efficacy of a coarse-to-fine method to protein structures.

Our main contributions are the following:

- **Deep Protein Autoencoding:** We introduce a new autoencoding model for protein sequence-structure representation, and offer an in-depth examination of its architecture through comprehensive ablation benchmarks. We showcase the unique effectiveness and versatility of our model’s latent geometric representations in structural latent interpolation tasks.
- **Neural Architecture for Proteins:** We propose novel learning algorithms for efficiently operating on all standard protein heavy atoms while preserving the natural permutation invariance of particular side-chain atoms. We introduce numerous methods for coarsening, refining and mixing of protein sequence-structure, employing irreducible representations of  $SO(3)$  to contract and spawn 3D coordinates directly from features.
- **All-Atom Protein Latent Diffusion:** We explore a novel generative approach to proteins by performing latent diffusion exclusively on geometric feature representations. We train

---

an efficient all-atom generative model for miniproteins, and provide diverse benchmarks to assess its performance.

## 2 BACKGROUND AND RELATED WORK

### 2.1 MODULARITY AND HIERARCHY IN PROTEINS

Protein sequences and structures display significant degrees of modularity. [Vallat et al. (2015)] introduces a library of common super-secondary structural motifs (Smotifs), while [Mackenzie et al. (2016)] shows protein structural space to be efficiently describable by small tertiary alphabets (TERMs). Motif-based methods have been successfully used in protein folding and design [Bystroff & Baker (1998); Li et al. (2022)].

### 2.2 SYMMETRIES IN NEURAL ARCHITECTURE FOR BIOMOLECULES

Learning algorithms greatly benefit from proactively exploiting symmetry structures present in their data domain [Bronstein et al. (2021); Smidt (2021)]. In this work, we investigate three relevant symmetries for the domain of protein structures:

**Euclidean Equivariance of Coordinates and Feature Representations.** Neural models equipped with roto-translational (Euclidean) invariance or equivariance have been shown to outperform competitors in molecular and point cloud tasks [Townshend et al. (2022); Miller et al. (2020); Deng et al. (2021)]. Similar results have been extensively reported across different structural tasks of protein modeling [Liu et al. (2022); Jing et al. (2021)]. Our proposed model takes advantage of Euclidean equivariance both in processing of coordinates and in its internal feature representations, which are composed of scalars and higher order geometric tensors [Thomas et al. (2018); Weiler et al. (2018)].

**Translation Equivariance of Sequence:** One-dimensional Convolutional Neural Networks (CNNs) have been demonstrated to successfully model protein sequences across a variety of tasks Karydis (2017); Hou et al. (2018); Lee et al. (2019); Yang et al. (2022). These models capture sequence-motif representations that are equivariant to translation of the sequence. However, sequential convolution is less common in architectures for protein structures, which are often cast as Graph Neural Networks (GNNs) [Zhang et al. (2021)]. Notably, [Fan et al. (2022)] proposes a CNN network to model the regularity of one-dimensional sequences along with three-dimensional structures, but they restrict their layout to coarsening. In this work, we further integrate geometry into sequence by directly using three-dimensional vector feature representations and transformations in 1D convolutions. We use this CNN to investigate an unsupervised autoencoding approach to protein structures.

**Permutation Invariances of Side-chain Atoms.** In order to capture the permutable ordering of atoms, neural models of molecules are often implemented with permutation-invariant GNNs [Wieder et al. (2020)]. Nevertheless, protein structures are sequentially ordered, and most standard side-chain atoms are readily orderable, with four exceptions of residues [Jumper et al. (2021)]. We use this fact to design an efficient approach to directly model all heavy atoms of proteins, proposing a method to parse atomic positions and symmetries through roto-translational equivariant features.

### 2.3 UNSUPERVISED LEARNING OF PROTEINS

Unsupervised techniques for capturing protein sequence and structure have witnessed remarkable advancements in recent years [Lin et al. (2023); Elnaggar et al. (2023); Zhang et al. (2022)]. Amongst unsupervised methods, autoencoder models learn to produce efficient low-dimensional representations using an informational bottleneck. These models have received significant attention for enabling learning of coarse representations of molecules [Wang & Gómez-Bombarelli (2019); Yang & Gómez-Bombarelli (2023); Winter et al. (2021); Wehmeyer & Noé (2018); Ramaswamy et al. (2021)], and have been successfully deployed to diverse protein tasks of modeling and sampling [Wang et al. (2022); Eguchi et al. (2020); Lin et al. (2021); Mansoor et al. (2023)].

---

## 2.4 DENOISING DIFFUSION FOR PROTEINS

Denoising Diffusion Probabilistic Models (DDPMs) [Sohl-Dickstein et al. (2015); Ho et al. (2020)] have found widespread adoption through diverse architectures for generative sampling of protein structures. Chroma [Ingraham et al. (2022)] trains random graph message passing through roto-translational invariant features, while RFDiffusion [Watson et al. (2022)] fine-tunes pretrained folding model RoseTTAFold [Baek et al. (2021a)] to denoising, employing SE(3)-equivariant transformers in structural decoding [Fuchs et al. (2020)]. [Yim et al. (2023); Anand & Achim (2022)] generalize denoising diffusion to frames of reference, employing Invariant Point Attention [Jumper et al. (2021)] to model three dimensions. More recently, [Fu et al. (2023)] designs a latent diffusion model by employing EGNNs [Satorras et al. (2022)] to contract the coordinate dimension into a smaller space. In contrast, our model uses *SO(3)-equivariant feature* representations to produce increasingly richer structural features from autoencoded coordinates. We perform generation directly on these features to demonstrate a latent diffusion generative model.

## 3 THE OPHIUCHUS ARCHITECTURE

We treat a protein as an ordered list  $(\mathbf{P}, \mathbf{V}^{0:l_{\max}})_{1:N}$  of  $N$  nodes, each with an anchoring position  $\mathbf{P}_i \in \mathbb{R}^{1 \times 3}$  and a collection of irreducible representations of  $SO(3)$ :  $\mathbf{V}_i^l \in \mathbb{R}^{d \times (2l+1)}$  for integers  $l \in [0, l_{\max}]$ ,  $i \in [1, N]$ . These representations are directly produced from sequence labels and all-atom positions, as we describe in the **Atom Encoder/Decoder** sections. Our model then acts with diverse operations on these representations. **Self-Interaction** updates vector representations independently, mixing within same-anchored vectors of different orders. In order to mix across the domain, **Sequence Convolution** updates  $K$ -sized windows of the list simultaneously, message-passing within sequence neighbors. Finally, **Spatial Convolutions** employ permutation invariant geometric messages to update the representations and coordinates of spatial neighbors. These modules are composed to build a coarsening-refining encoder-decoder hourglass architecture.

### 3.1 ALL-ATOM ATOM ENCODER AND DECODER

The input format of our modeling starts at the residue level. Given a particular  $i$ -th residue, let  $\mathbf{R}_i \in \mathcal{R}$  denote its residue label,  $\mathbf{P}_i^\alpha \in \mathbb{R}^{1 \times 3}$  denote the global position of its alpha carbon ( $\mathbf{C}_\alpha$ ), and  $\mathbf{P}_i^*$  the position of all other heavy atoms relative to  $\mathbf{C}_\alpha$ . We produce initial residue representations  $(\mathbf{P}, \mathbf{V}^{0:l_{\max}})_i^0$  by setting anchors  $\mathbf{P}_i^0 = \mathbf{P}_i^\alpha$ , scalar representations  $\mathbf{P}_i^{0,l=0} = \text{Embed}(\mathbf{R}_i)$ , and vector representations  $\mathbf{V}_i^{0,l>0}$  to explicitly encode relative atomic positions  $\mathbf{P}_i^*$ . In particular, provided the residue label  $\mathbf{R}_i$ , heavy atoms of most standard protein residues are readily orderable and may be directly processed as a stack of  $\mathbf{V}^{l=1}$  relative vector positions.

However, some of the standard residues do present two-permutations within their atom configurations (i.e. they are not orderable). To handle these cases, we map the set of two relative vectors into a pair  $(\mathbf{V}^{l=1}, \mathbf{V}^{l=2})$  where  $\mathbf{V}^{l=1}$  is the center and  $\mathbf{V}^{l=2}$  is the unsigned difference. This signal is invariant to corresponding atomic two-flips, while still carrying relevant information on positioning and angularity. Decoding is handled similarly. Refer to Appendix A for further details.

---

#### Algorithm 1: ALL-ATOM ENCODING

**Input:**  $\mathbf{C}_\alpha$  Position  $\mathbf{P}^\alpha \in \mathbb{R}^{1 \times 3}$   
**Input:** Heavy Atom Relative Positions  $\mathbf{P}^* \in \mathbb{R}^{n \times 3}$   
**Input:** Residue Label  $\mathbf{R} \in \mathcal{R}$   
**Output:** Latent Representation  $(\mathbf{P}, \mathbf{V}^{l=0:2})$   
 $\mathbf{P} \leftarrow \mathbf{P}^\alpha$   
 $\mathbf{V}^{l=0} \leftarrow \text{Embed}(\mathbf{R})$   
 $\mathbf{V}^{l=1} \leftarrow \text{UnorderableCenters}(\mathbf{R}, \mathbf{P}^*)$   
 $\mathbf{V}^{l=2} \leftarrow \text{UnorderableDifferences}(\mathbf{R}, \mathbf{P}^*)$   
 $\mathbf{V}^{l=1} \leftarrow \mathbf{V}^{l=1} \oplus \text{Orderable}(\mathbf{R}, \mathbf{P}^*)$   
**return**  $(\mathbf{P}, \mathbf{V}^{l=0:2})$

---



---

#### Algorithm 2: ALL-ATOM DECODING

**Input:** Latent Representation  $(\mathbf{P}, \mathbf{V}^{l=0:2})$   
**Output:**  $\mathbf{C}_\alpha$  Position  $\mathbf{P}^\alpha \in \mathbb{R}^{1 \times 3}$   
**Output:** Heavy Atom Relative Positions  $\mathbf{P}^* \in \mathbb{R}^{n \times 3}$   
**Output:** Residue Label  $\mathbf{R} \in \mathcal{R}$   
 $\mathbf{P}^\alpha \leftarrow \mathbf{P}$   
 $\mathbf{R} \leftarrow \text{Softmax}(\mathbf{V}^{l=0})$   
 $\mathbf{P}^* \leftarrow \text{Orderable}(\mathbf{R}, \mathbf{V}^{l=1})$   
 $\mathbf{P}^* \leftarrow \mathbf{P}^* \oplus \text{Unorderable}(\mathbf{R}, \mathbf{V}^{l=1}, \mathbf{V}^{l=2})$   
**return**  $(\mathbf{P}^\alpha, \mathbf{P}^*, \mathbf{R})$

---

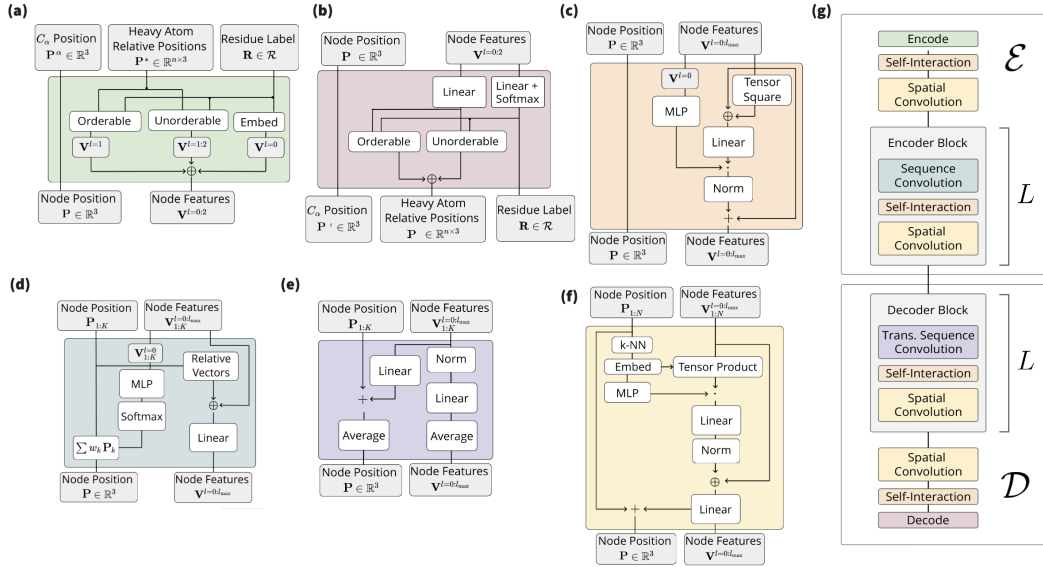


Figure 2: **Building Blocks of Ophiuchus:** (a) **Atom Encoder** and (b) **Atom Decoder** enable the model to directly take and produce atomic coordinates. (c) **Self Interaction** updates representations internally, across different vector orders  $l$ . (d) **Sequence Convolution** and (e) **Transpose Sequence Convolution** communicate sequence neighbors and produce coarser and finer representations, respectively. (d) **Spatial Convolution** interacts spatial neighbors. (g) **Hourglass model:** we compose those modules to build encoder and decoder models, stacking them into an autoencoder.

This processing makes Ophiuchus strictly blind to ordering flips within permutable atoms, while still enabling it to operate directly on all heavy atoms in an efficient, stacked representation.

### 3.2 SELF-INTERACTION

Our Self-Interaction transform draws inspiration from MACE [Batatia et al. (2022)]. This transformation updates the feature vectors  $\mathbf{V}_i^{0:l_{\max}}$  localized at the same anchoring node  $i$ . Importantly, it blends feature vectors  $\mathbf{V}^l$  of varying orders  $l$  by employing tensor products of the features with themselves. We offer two implementations of these tensor products to cater to different computational needs. For a comprehensive explanation, please refer to Appendix B.

---

#### Algorithm 3: Self-Interaction

---

**Input:** Latent Representation  $(\mathbf{P}, \mathbf{V}^{0:l_{\max}})$

$\tilde{\mathbf{V}}^{0:l_{\max}} \leftarrow \mathbf{V}^{0:l_{\max}}$	▷ Save For Later
$\mathbf{V}^{0:l_{\max}} \leftarrow \mathbf{V}^{0:l_{\max}} \oplus (\mathbf{V}^{0:l_{\max}})^{\otimes 2}$	▷ Tensor Product with itself
$\mathbf{V}^{0:l_{\max}} \leftarrow \text{Linear}(\mathbf{V}^{0:l_{\max}})$	
$\mathbf{V}^{0:l_{\max}} \leftarrow \text{MLP}(\mathbf{V}^{l=0}) \cdot \mathbf{V}^{0:l_{\max}}$	▷ Scalar-Irrep Multiplication
$\mathbf{V}^{0:l_{\max}} \leftarrow \mathbf{V}^{0:l_{\max}} + \tilde{\mathbf{V}}^{0:l_{\max}}$	▷ If the Multiplicities Match
$\mathbf{V}^{0:l_{\max}} \leftarrow \text{Norm}(\mathbf{V}^{0:l_{\max}})$	▷ Normalize $l$ -Wise

**return**  $(\mathbf{P}, \mathbf{V}^{0:l_{\max}})$

---

### 3.3 SEQUENCE CONVOLUTION

We introduce a one-dimensional roto-translational equivariant convolutional kernel designed to operate on representations of  $\text{SO}(3)$  and  $\mathbb{R}^3$ . Given a kernel window size  $K$  and stride  $S$ , we concatenate representations  $\mathbf{V}_{i-\frac{K}{2}:i+\frac{K}{2}}^{0:l_{\max}}$  with the same  $l$  value. Additionally, we include normalized relative vectors between anchoring positions  $\mathbf{P}_{i-\frac{K}{2}:i+\frac{K}{2}}$ . Following conventional CNN architectures, this

concatenated representation undergoes a linear transformation. The scalars in the resulting representation are then converted into weights, which are used to combine window coordinates into a new coordinate. To ensure translational equivariance, these weights are constrained to sum to one.

---

**Algorithm 4:** Sequence Convolution

---

**Input:** Window of Latent Representations  $(\mathbf{P}, \mathbf{V}^{0:l_{\max}})_{1:K}$   
 $w_{1:K} \leftarrow \text{Softmax}\left(\text{MLP}\left(\mathbf{V}_{1:K}^0\right)\right)$  ▷ Such that  $\sum_k w_k = 1$   
 $\mathbf{P} \leftarrow \sum_{k=1}^K w_k \mathbf{P}_k$   
 $\tilde{\mathbf{P}}_{1:K,1:K} \leftarrow \bigoplus_{i,j} \frac{\mathbf{P}_i - \mathbf{P}_j}{\|\mathbf{P}_i - \mathbf{P}_j\|}$  ▷ All relative vectors  
 $\mathbf{V}^{0:l_{\max}} \leftarrow \text{Linear}\left(\mathbf{V}_{1:K}^{0:l_{\max}} \oplus \tilde{\mathbf{P}}_{1:K,1:K}\right)$   
**return**  $(\mathbf{P}, \mathbf{V}^{0:l_{\max}})$

---

When  $S > 1$ , sequence convolutions reduce the dimensionality along the sequence axis, yielding mixed representations and coarse coordinates. To reverse this process, we introduce a transpose convolution algorithm that geometrically reconstructs both the sequence and its positional coordinates. For further details, please refer to Appendix C.

### 3.4 SPATIAL CONVOLUTION

Spatial convolutions update representations through message passing within  $k$ -nearest spatial neighbors. Message representations incorporate  $\text{SO}(3)$  signals from the vector difference between neighbor coordinates, and we aggregate messages with permutation-invariant means. After aggregation, we linearly transform the vector representations into a single vector that is used to update the coordinates.

---

**Algorithm 5:** Spatial Convolution

---

**Input:** Latent Representations  $(\mathbf{P}, \mathbf{V}^{0:l_{\max}})_{1:N}$   
**Input:** Output Node Index  $i$   
 $\hat{\mathbf{V}}^{0:l_{\max}} \leftarrow \mathbf{V}_i^{0:l_{\max}}$  ▷ Save for Later  
 $(\tilde{\mathbf{P}}, \tilde{\mathbf{V}}^{0:l_{\max}})_{1:k} \leftarrow k\text{-Nearest-Neighbors}(\mathbf{P}_i, \mathbf{P}_{1:N})$   
 $(\phi, R, u)_{1:k} \leftarrow \text{Embeddings}(\tilde{\mathbf{X}}_{1:k} - \mathbf{P}_i)$  ▷ Angular/Radial Embeddings  
 $\mathbf{V}^{0:l_{\max}} \leftarrow \text{Linear}\left(\left(\sum_k u_k \text{MLP}(R_k) \tilde{\mathbf{V}}_k^{0:l_{\max}} \otimes \phi_k\right) / \left(\sum_k u_k\right)\right)$   
 $\mathbf{V}^{0:l_{\max}} \leftarrow \text{Norm}\left(\mathbf{V}^{0:l_{\max}}\right)$  ▷ Normalize  $l$ -Wise  
 $\mathbf{V}^{0:l_{\max}} \leftarrow \text{Linear}\left(\mathbf{V}^{0:l_{\max}} \oplus \hat{\mathbf{V}}^{0:l_{\max}}\right)$   
 $\mathbf{P} \leftarrow \mathbf{P}_i + 10^{-3} \text{Linear}\left(\mathbf{V}^{l=1}\right)$   
**return**  $(\mathbf{P}, \mathbf{V}^{0:l_{\max}})$

---

### 3.5 DEEP COARSENING AUTOENCODER

We compose Space Convolution, Self-Interaction and Sequence Convolution modules to define a coarsening/refining block. The block mixes representations across all relevant axes of the domain while producing coarsened, downsampled positions and mixed embeddings. The reverse result – finer positions and decoupled embeddings – is achieved by changing the standard Sequence Convolution to its transpose counterpart. When employing sequence convolutions of stride  $S > 1$ , we increase the dimensionality of the feature representation according to a rescaling factor hyperparameter (Table 1). We stack  $L$  coarsening blocks to build a deep neural encoder  $\mathcal{E}$ , and symmetrically  $L$  refining blocks to build a decoder  $\mathcal{D}$ .

### 3.6 RECONSTRUCTION LOSSES

We use a number of reconstruction losses to ensure good quality of produced proteins.

**Vector Map Loss.** We train the model by directly comparing internal three-dimensional vector difference maps. Let  $V(\mathbf{P})$  denote the internal vector map between all atoms  $\mathbf{P}$  in our data, that is,  $V(\mathbf{P})^{i,j} = (\mathbf{P}^i - \mathbf{P}^j) \in \mathbb{R}^{N \times N \times 3}$ . We then directly minimize  $\text{HuberLoss}(V(\mathbf{P}), V(\hat{\mathbf{P}}))$  [Huber (1992)].

**Cross Entropy Loss.** We train the model to predict logits over alphabet  $\mathcal{R}$  per residue. We then minimize the cross entropy between predicted logits and ground labels.

**Chemical Losses.** We incorporate  $L_2$ -norm losses for comparing bonds, angles and dihedrals between prediction and ground truth. For nonbonded atoms, a clash loss is evaluated using standard Van der Waals atomic radii.

An additional stage is employed for processing permutation symmetry breaks. Please refer to Appendix D for further details.

### 3.7 IMPLEMENTATION

We train all models on single-GPU A6000 and GTX-1080 Ti machines. We implement Ophiuchus in Jax using the python libraries e3nn-jax [Geiger & Smidt (2022)] and Haiku [Hennigan et al. (2020)].

## 4 METHODS AND RESULTS

### 4.1 ARCHITECTURE ABLATION

To investigate the effects of different architecture layouts and coarsening rates, we train different instantiations of Ophiuchus to coarsen representations of contiguous 160-sized protein fragments from the Protein Databank (PDB) [Berman et al. (2000)]. We filter out entries tagged with resolution higher than 2.5 Å, and total sequence lengths larger than 512. We also ensure proteins in the dataset have same chirality. For ablations, the sequence convolution uses kernel size of 5 and stride 3, channel rescale factor per layer is one of {1.5, 1.7, 2.0}, and the number of downsampling layers ranges in 3-5. The initial residue representation uses 16 channels, where each channel is composed of one scalar ( $l = 0$ ) and one 3D vector ( $l = 1$ ). All experiments were repeated 3 times with different initialization seeds and data shuffles.

Table 1: **Autoencoder Recovery from Compressed Representations**

Downsampling Factor	Channels/Layer	# Params [1e6]	C $\alpha$ -RMSD (Å)	All-Atom RMSD (Å)	GDT-TS	GDT-HA	Residue Acc. (%)
17	[16, 24, 36]	0.34	0.90 ± 0.20	0.68 ± 0.08	94 ± 3	76 ± 4	97 ± 2
17	[16, 27, 45]	0.38	0.89 ± 0.21	0.70 ± 0.09	94 ± 3	77 ± 5	98 ± 1
17	[16, 32, 64]	0.49	1.02 ± 0.25	0.72 ± 0.09	92 ± 4	73 ± 5	98 ± 1
53	[16, 24, 36, 54]	0.49	1.03 ± 0.18	0.83 ± 0.10	91 ± 3	72 ± 5	60 ± 4
53	[16, 27, 45, 76]	0.67	0.92 ± 0.19	0.77 ± 0.09	93 ± 3	75 ± 5	66 ± 4
53	[16, 32, 64, 128]	1.26	1.25 ± 0.32	0.80 ± 0.16	86 ± 5	65 ± 6	67 ± 5
160	[16, 24, 36, 54, 81]	0.77	1.67 ± 0.24	1.81 ± 0.16	77 ± 4	54 ± 5	17 ± 3
160	[16, 27, 45, 76, 129]	1.34	1.39 ± 0.23	1.51 ± 0.17	83 ± 4	60 ± 5	17 ± 3
160	[16, 32, 64, 128, 256]	3.77	1.21 ± 0.25	1.03 ± 0.15	87 ± 5	65 ± 6	27 ± 4

In our experiments we find a trade-off between domain coarsening factor and reconstruction performance. In Table 1 we show that although residue recovery suffers from large downsampling factors, structure recovery rates remain comparable between various settings. Moreover, we find that we are able to model all heavy atoms in proteins, as opposed to only C $\alpha$  atoms (as commonly done), and still recover the structure with high precision. These results demonstrate that protein data can be captured effectively and efficiently using sequence-modular geometric representations. We directly utilize the learned compact latent space as shown below by various examples. For further ablation analysis please refer to Appendix F.

### 4.2 LATENT CONFORMATIONAL INTERPOLATION

To demonstrate the power of Ophiuchus’s geometric latent space, we show smooth interpolation between two states of a protein structure without explicit latent regularization [Ramaswamy et al. (2021)]. We utilize PDBFlex dataset [Hrabe et al. (2016)] to pick pairs of flexible conformational

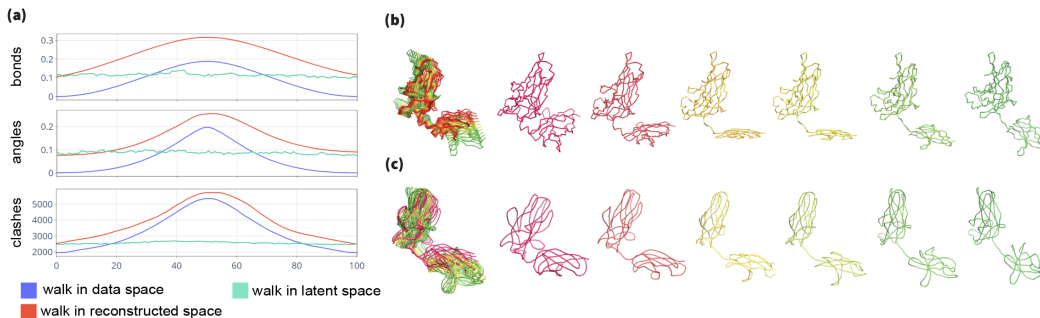


**Figure 3: Latent Conformational Interpolation.** (a) Comparison of chemical validity metrics across interpolated structures of Nuclear Factor of Activated T-Cell (NFAT) Protein (PDB ID: 1S9K and PDB ID: 2O93). We plot results for interpolations on the original data space, on the latent space, and on the autoencoder-reconstructed data space. We note that near interpolation endpoints, latent and AE-reconstructed interpolations perform worse than direct interpolations. This is expected and is a result of the low resolution decoding of the AE. However, only for the latent interpolation the chemical deviation stays consistent, demonstrating that our latent space compactly and smoothly represents the protein space. (b) Linear interpolation of coordinates between two conformational endpoints. (c) Decoded linear latent interpolation between the same encoded states as in (b).

snapshots of a protein. We utilize these pairs as endpoints for our interpolation. We train a large Ophiuchus reconstruction model on general PDB data. The model coarsens up to 485-residue proteins into a single high-order geometric representation using 6 convolutional downsampling layers each with kernel size 5 and stride 3. The endpoint structures are compressed into single high-order geometric representation to enable direct latent interpolation. We then compare the results of linear interpolation in this *latent* space against linear interpolation in the coordinate domain (Fig. 3). To determine chemical validity of intermediate states, we scan protein data to quantify average bond lengths and inter-bond angles. We then calculate  $L_2$  deviation of bonds and angles of interpolated structures. Additionally, we measure atomic clashes by counting collisions of van der Waals radii of non-bonded atoms. Our experiment shows that the decoded structures from latent interpolation maintain a consistent profile of chemical validity, while direct interpolation in the coordinate domain disrupts it significantly. We provide an additional example in Appendix G.

### 4.3 LATENT DIFFUSION

We investigate the performance of a generative model trained on the Ophiuchus latent space for sampling decodable protein structure representations. We leverage the miniprotein dataset produced by [Cao et al. (2022)] for protein binder design. The dataset consists of 66k all-atom structures of sequence length between 50 and 65, and composes of diverse folds and sequences across 5 secondary structure topologies. The small sequence sizes facilitate precise reconstruction from unified bottlenecks, enabling a generation method exclusively on latent feature representations to implicitly generate *all-atom* coordinates.

To that end, we employ DDPMs [Ho et al. (2020); Sohl-Dickstein et al. (2015)] on signals over  $SO(3)$  to produce decodable embeddings. First, we train deep autoencoder models for backbone and all-atom structures over the miniprotein dataset. In order to ensure that bottleneck representations  $\mathbf{Z}_0$  are well-behaved targets for generation, we further regularize the latent space. We build a denoising network by stacking  $L_D = 7$  layers of the Ophiuchus Self-Interaction Fig. (4.a). We parameterize the diffusion model following [Salimans & Ho (2022)], and train it to recover  $\mathbf{Z}_0$  from  $\mathbf{Z}_t$ :  $\mathcal{L}_{\text{diffusion}} = \mathbb{E}_{\epsilon, t} [w(\lambda_t) \|\hat{\mathbf{Z}}_0(\mathbf{Z}_t) - \mathbf{Z}_0\|_2^2]$ . (Appendix H)

In Fig.(5.b) we show the distribution of TM-scores for joint sampling of sequence and all-atom structure by the diffusion model. We produce marginal distributions of generated samples Fig.(5.e) and find them to successfully approximate the densities of ground truth data. To test the robustness of joint sampling of structure and sequence, we compute self-consistency TM-Scores[Trippe et al. (2023)]. 54% of our sampled backbones have scTM scores  $> 0.5$  compared to 77.6% of samples from

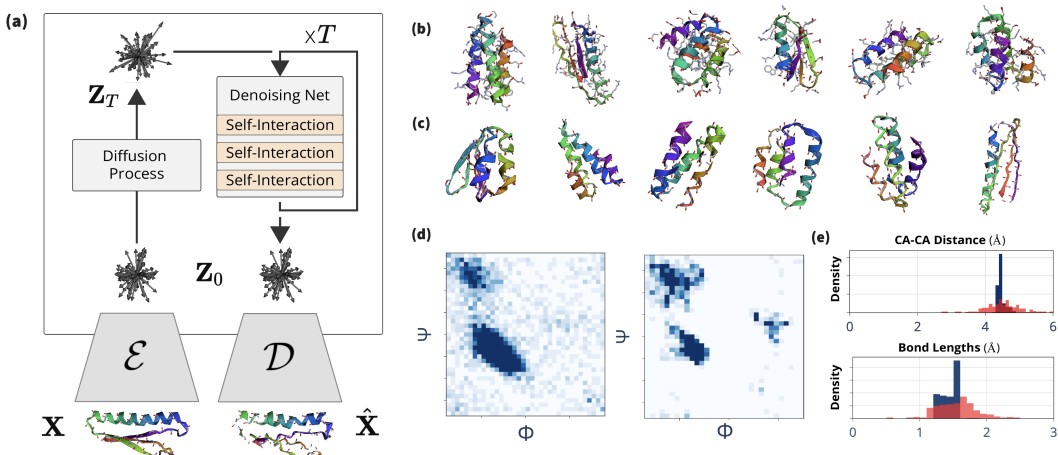


Figure 4: **All-Atom Protein Latent Diffusion.** (a) We attach a diffusion process to Ophiuchus representations and learn a denoising network to sample embeddings of  $SO(3)$  that decode to all-atom protein structures. (b) Random samples from all-atom model. (c) Random samples from backbone model. (d) Ramachandran plots of sampled (left) and ground (right) distributions. (e) Comparison of  $C\alpha$ - $C\alpha$  distances and all-atom bond lengths between learned (red) and ground (blue) distributions.

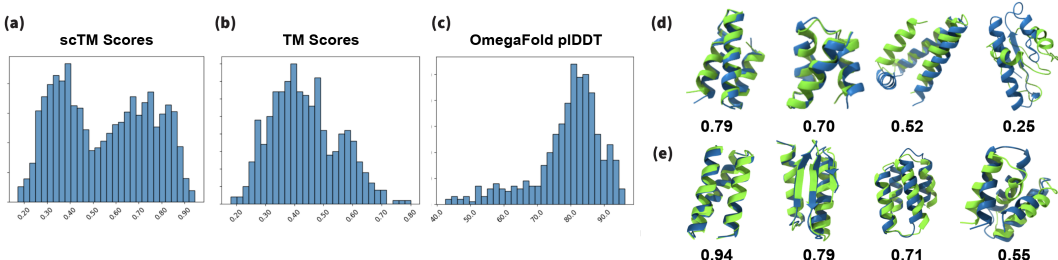


Figure 5: **Self-Consistency Template Matching Scores for Ophiuchus Diffusion.** (a) Distribution of scTM scores for 500 sampled backbone. (b) Distribution of TM-Scores of jointly sampled backbones and sequences from an all-atom diffusion model and corresponding OmegaFold models.(c) Distribution of average pLDDT scores for 500 sampled backbones (d) TM-Score between sampled backbone(green) and OmegaFold structure(blue) (e) TM-Score between sampled backbone(green) and the most confident OmegaFold structure of the sequence recovered from ProteinMPNN (blue)

RFDiffusion. We also sample a protein between 50-65 amino acids in an average 0.21s compared to 11s taken by RFDiffusion on a RTX A6000. Details can be found in Appendix H.

## 5 CONCLUSION AND FUTURE WORK

In this work, we introduced a new unsupervised autoencoder model for protein structure and sequence representation. Through extensive ablation on its architecture, we quantified the trade-offs between model complexity and representation quality. We demonstrated the power of our learned representations in latent interpolation, and investigated its usage as basis for efficient latent generation of all-atom proteins. Our studies suggest Ophiuchus to provide a strong foundation for constructing state-of-the-art protein neural architectures. In future work, we will investigate scaling Ophiuchus representations and generation to larger proteins and additional molecular domains.

---

## REFERENCES

- Namrata Anand and Tudor Achim. Protein structure and sequence generation with equivariant denoising diffusion probabilistic models, 2022.
- Minkyung Baek, Frank DiMaio, Ivan Anishchenko, Justas Dauparas, Sergey Ovchinnikov, Gyu Rie Lee, Jue Wang, Qian Cong, Lisa N. Kinch, R. Dustin Schaeffer, Claudia Millán, Hahnbeom Park, Carson Adams, Caleb R. Glassman, Andy DeGiovanni, Jose H. Pereira, Andria V. Rodrigues, Alberdina A. van Dijk, Ana C. Ebrecht, Diederik J. Opperman, Theo Sagmeister, Christoph Buhlheller, Tea Pavkov-Keller, Manoj K. Rathinaswamy, Udit Dalwadi, Calvin K. Yip, John E. Burke, K. Christopher Garcia, Nick V. Grishin, Paul D. Adams, Randy J. Read, and David Baker. Accurate prediction of protein structures and interactions using a three-track neural network. *Science*, 373(6557):871–876, August 2021a. doi: 10.1126/science.abj8754. URL <https://doi.org/10.1126/science.abj8754>.
- Minkyung Baek, Frank DiMaio, Ivan Anishchenko, Justas Dauparas, Sergey Ovchinnikov, Gyu Rie Lee, Jue Wang, Qian Cong, Lisa N Kinch, R Dustin Schaeffer, et al. Accurate prediction of protein structures and interactions using a three-track neural network. *Science*, 373(6557):871–876, 2021b.
- Ilyes Batatia, David Peter Kovacs, Gregor N. C. Simm, Christoph Ortner, and Gabor Csanyi. MACE: Higher order equivariant message passing neural networks for fast and accurate force fields. In Alice H. Oh, Alekh Agarwal, Danielle Belgrave, and Kyunghyun Cho (eds.), *Advances in Neural Information Processing Systems*, 2022. URL <https://openreview.net/forum?id=YpP5ngE-ZU>.
- Helen M Berman, John Westbrook, Zukang Feng, Gary Gilliland, Talapady N Bhat, Helge Weissig, Ilya N Shindyalov, and Philip E Bourne. The protein data bank. *Nucleic acids research*, 28(1): 235–242, 2000.
- Michael M. Bronstein, Joan Bruna, Taco Cohen, and Petar Velickovic. Geometric deep learning: Grids, groups, graphs, geodesics, and gauges. *CoRR*, abs/2104.13478, 2021. URL <https://arxiv.org/abs/2104.13478>.
- Christopher Bystroff and David Baker. Prediction of local structure in proteins using a library of sequence-structure motifs. *Journal of molecular biology*, 281(3):565–577, 1998.
- Longxing Cao, Brian Coventry, Inna Goreschnik, Buwei Huang, William Sheffler, Joon Sung Park, Kevin M Jude, Iva Marković, Rameshwar U Kadam, Koen HG Verschueren, et al. Design of protein-binding proteins from the target structure alone. *Nature*, 605(7910):551–560, 2022.
- Congyue Deng, Or Litany, Yueqi Duan, Adrien Poulénard, Andrea Tagliasacchi, and Leonidas Guibas. Vector neurons: A general framework for so(3)-equivariant networks, 2021.
- Raphael R. Eguchi, Christian A. Choe, and Po-Ssu Huang. Ig-VAE: Generative modeling of protein structure by direct 3d coordinate generation. *PLOS Computational Biology*, August 2020. doi: 10.1101/2020.08.07.242347. URL <https://doi.org/10.1101/2020.08.07.242347>.
- Ahmed Elnaggar, Hazem Essam, Wafaa Salah-Eldin, Walid Moustafa, Mohamed Elkerdawy, Charlotte Rochereau, and Burkhard Rost. Ankh: Optimized protein language model unlocks general-purpose modelling, 2023.
- Hehe Fan, Zhangyang Wang, Yi Yang, and Mohan Kankanhalli. Continuous-discrete convolution for geometry-sequence modeling in proteins. In *The Eleventh International Conference on Learning Representations*, 2022.
- Cong Fu, Keqiang Yan, Limei Wang, Wing Yee Au, Michael McThrow, Tao Komikado, Koji Maruhashi, Kanji Uchino, Xiaoning Qian, and Shuiwang Ji. A latent diffusion model for protein structure generation, 2023.
- Fabian B. Fuchs, Daniel E. Worrall, Volker Fischer, and Max Welling. Se(3)-transformers: 3d rotation equivariant attention networks, 2020.
- Mario Geiger and Tess Smidt. e3nn: Euclidean neural networks, 2022.

- 
- Tom Hennigan, Trevor Cai, Tamara Norman, Lena Martens, and Igor Babuschkin. Haiku: Sonnet for JAX, 2020. URL <http://github.com/deepmind/dm-haiku>.
- Jonathan Ho, Ajay Jain, and Pieter Abbeel. Denoising diffusion probabilistic models, 2020.
- Jie Hou, Badri Adhikari, and Jianlin Cheng. Deepsf: deep convolutional neural network for mapping protein sequences to folds. *Bioinformatics*, 34(8):1295–1303, 2018.
- Thomas Hrabe, Zhanwen Li, Mayya Sedova, Piotr Rotkiewicz, Lukasz Jaroszewski, and Adam Godzik. Pdbflex: exploring flexibility in protein structures. *Nucleic acids research*, 44(D1): D423–D428, 2016.
- Peter J Huber. Robust estimation of a location parameter. In *Breakthroughs in statistics: Methodology and distribution*, pp. 492–518. Springer, 1992.
- John Ingraham, Max Baranov, Zak Costello, Vincent Frappier, Ahmed Ismail, Shan Tie, Wujie Wang, Vincent Xue, Fritz Obermeyer, Andrew Beam, and Gevorg Grigoryan. Illuminating protein space with a programmable generative model. *bioRxiv*, December 2022. doi: 10.1101/2022.12.01.518682. URL <https://doi.org/10.1101/2022.12.01.518682>.
- Bowen Jing, Stephan Eismann, Patricia Suriana, Raphael J. L. Townshend, and Ron Dror. Learning from protein structure with geometric vector perceptrons, 2021.
- John Jumper, Richard Evans, Alexander Pritzel, Tim Green, Michael Figurnov, Olaf Ronneberger, Kathryn Tunyasuvunakool, Russ Bates, Augustin Žídek, Anna Potapenko, et al. Highly accurate protein structure prediction with alphafold. *Nature*, 596(7873):583–589, 2021.
- Thrasylvoulos Karydis. *Learning hierarchical motif embeddings for protein engineering*. PhD thesis, Massachusetts Institute of Technology, 2017.
- Sebastian Kmiecik, Dominik Gront, Michal Kolinski, Lukasz Wieteska, Aleksandra Elzbieta Dawid, and Andrzej Kolinski. Coarse-grained protein models and their applications. *Chemical reviews*, 116(14):7898–7936, 2016.
- Ingoo Lee, Jongsoo Keum, and Hojung Nam. Deepconv-dti: Prediction of drug-target interactions via deep learning with convolution on protein sequences. *PLoS computational biology*, 15(6): e1007129, 2019.
- Alex J. Li, Vikram Sundar, Gevorg Grigoryan, and Amy E. Keating. Terminator: A neural framework for structure-based protein design using tertiary repeating motifs, 2022.
- Yeqing Lin and Mohammed AlQuraishi. Generating novel, designable, and diverse protein structures by equivariantly diffusing oriented residue clouds, 2023.
- Zeming Lin, Tom Sercu, Yann LeCun, and Alexander Rives. Deep generative models create new and diverse protein structures. In *Machine Learning for Structural Biology Workshop, NeurIPS*, 2021.
- Zeming Lin, Halil Akin, Roshan Rao, Brian Hie, Zhongkai Zhu, Wenting Lu, Nikita Smetanin, Robert Verkuil, Ori Kabeli, Yaniv Shmueli, et al. Evolutionary-scale prediction of atomic-level protein structure with a language model. *Science*, 379(6637):1123–1130, 2023.
- David D Liu, Ligia Melo, Allan Costa, Martin Vögele, Raphael JL Townshend, and Ron O Dror. Euclidean transformers for macromolecular structures: Lessons learned. *2022 ICML Workshop on Computational Biology*, 2022.
- Craig O Mackenzie and Gevorg Grigoryan. Protein structural motifs in prediction and design. *Current opinion in structural biology*, 44:161–167, 2017.
- Craig O. Mackenzie, Jianfu Zhou, and Gevorg Grigoryan. Tertiary alphabet for the observable protein structural universe. *Proceedings of the National Academy of Sciences*, 113(47), November 2016. doi: 10.1073/pnas.1607178113. URL <https://doi.org/10.1073/pnas.1607178113>.

- 
- Sanaa Mansoor, Minkyung Baek, Hahnbeom Park, Gyu Rie Lee, and David Baker. Protein ensemble generation through variational autoencoder latent space sampling. *bioRxiv*, pp. 2023–08, 2023.
- Benjamin Kurt Miller, Mario Geiger, Tess E. Smidt, and Frank Noé. Relevance of rotationally equivariant convolutions for predicting molecular properties. *CoRR*, abs/2008.08461, 2020. URL <https://arxiv.org/abs/2008.08461>.
- Chris Olah, Arvind Satyanarayan, Ian Johnson, Shan Carter, Ludwig Schubert, Katherine Ye, and Alexander Mordvintsev. The building blocks of interpretability. *Distill*, 2018. doi: 10.23915/distill.00010. <https://distill.pub/2018/building-blocks>.
- Venkata K Ramaswamy, Samuel C Musson, Chris G Willcocks, and Matteo T Degiacomi. Deep learning protein conformational space with convolutions and latent interpolations. *Physical Review X*, 11(1):011052, 2021.
- Tim Salimans and Jonathan Ho. Progressive distillation for fast sampling of diffusion models, 2022.
- Victor Garcia Satorras, Emiel Hoogetboom, and Max Welling. E(n) equivariant graph neural networks, 2022.
- Tess E Smidt. Euclidean symmetry and equivariance in machine learning. *Trends in Chemistry*, 3(2):82–85, 2021.
- Jascha Sohl-Dickstein, Eric A. Weiss, Niru Maheswaranathan, and Surya Ganguli. Deep unsupervised learning using nonequilibrium thermodynamics, 2015.
- Sebastian Swanson, Venkatesh Sivaraman, Gevorg Grigoryan, and Amy E Keating. Tertiary motifs as building blocks for the design of protein-binding peptides. *Protein Science*, 31(6):e4322, 2022.
- Nathaniel Thomas, Tess Smidt, Steven Kearnes, Lusann Yang, Li Li, Kai Kohlhoff, and Patrick Riley. Tensor field networks: Rotation- and translation-equivariant neural networks for 3d point clouds, 2018.
- Raphael J. L. Townshend, Martin Vögele, Patricia Suriana, Alexander Derry, Alexander Powers, Yianni Laloudakis, Sidhika Balachandar, Bowen Jing, Brandon Anderson, Stephan Eismann, Risi Kondor, Russ B. Altman, and Ron O. Dror. Atom3d: Tasks on molecules in three dimensions, 2022.
- Brian L. Trippe, Jason Yim, Doug Tischer, David Baker, Tamara Broderick, Regina Barzilay, and Tommi Jaakkola. Diffusion probabilistic modeling of protein backbones in 3d for the motif-scaffolding problem, 2023.
- Brinda Vallat, Carlos Madrid-Aliste, and Andras Fiser. Modularity of protein folds as a tool for template-free modeling of structures. *PLoS computational biology*, 11(8):e1004419, 2015.
- Wujie Wang and Rafael Gómez-Bombarelli. Coarse-graining auto-encoders for molecular dynamics. *npj Computational Materials*, 5(1):125, 2019.
- Wujie Wang, Minkai Xu, Chen Cai, Benjamin Kurt Miller, Tess Smidt, Yusu Wang, Jian Tang, and Rafael Gómez-Bombarelli. Generative coarse-graining of molecular conformations, 2022.
- Joseph L. Watson, David Juergens, Nathaniel R. Bennett, Brian L. Trippe, Jason Yim, Helen E. Eisenach, Woody Ahern, Andrew J. Borst, Robert J. Ragotte, Lukas F. Milles, Basile I. M. Wicky, Nikita Hanikel, Samuel J. Pellock, Alexis Courbet, William Sheffler, Jue Wang, Preetham Venkatesh, Isaac Sappington, Susana Vázquez Torres, Anna Lauko, Valentin De Bortoli, Emile Mathieu, Regina Barzilay, Tommi S. Jaakkola, Frank DiMaio, Minkyung Baek, and David Baker. Broadly applicable and accurate protein design by integrating structure prediction networks and diffusion generative models. *bioRxiv*, 2022. doi: 10.1101/2022.12.09.519842. URL <https://www.biorxiv.org/content/early/2022/12/10/2022.12.09.519842>.
- Christoph Wehmeyer and Frank Noé. Time-lagged autoencoders: Deep learning of slow collective variables for molecular kinetics. *The Journal of Chemical Physics*, 148(24), mar 2018. doi: 10.1063/1.5011399. URL <https://doi.org/10.1063%2F1.5011399>.

- 
- Maurice Weiler, Mario Geiger, Max Welling, Wouter Boomsma, and Taco Cohen. 3d steerable cnns: Learning rotationally equivariant features in volumetric data, 2018.
- Oliver Wieder, Stefan Kohlbacher, Méline Kuenemann, Arthur Garon, Pierre Ducrot, Thomas Seidel, and Thierry Langer. A compact review of molecular property prediction with graph neural networks. *Drug Discovery Today: Technologies*, 37:1–12, 2020.
- Robin Winter, Frank Noé, and Djork-Arné Clevert. Auto-encoding molecular conformations, 2021.
- Ruidong Wu, Fan Ding, Rui Wang, Rui Shen, Xiwen Zhang, Shitong Luo, Chenpeng Su, Zuofan Wu, Qi Xie, Bonnie Berger, et al. High-resolution de novo structure prediction from primary sequence. *BioRxiv*, pp. 2022–07, 2022.
- Kevin K Yang, Nicolo Fusi, and Alex X Lu. Convolutions are competitive with transformers for protein sequence pretraining. *bioRxiv*, pp. 2022–05, 2022.
- Soojung Yang and Rafael Gómez-Bombarelli. Chemically transferable generative backmapping of coarse-grained proteins, 2023.
- Jason Yim, Brian L. Trippe, Valentin De Bortoli, Emile Mathieu, Arnaud Doucet, Regina Barzilay, and Tommi Jaakkola. Se(3) diffusion model with application to protein backbone generation, 2023.
- Xiao-Meng Zhang, Li Liang, Lin Liu, and Ming-Jing Tang. Graph neural networks and their current applications in bioinformatics. *Frontiers in genetics*, 12:690049, 2021.
- Zuobai Zhang, Minghao Xu, Arian Jamasb, Vijil Chenthamarakshan, Aurelie Lozano, Payel Das, and Jian Tang. Protein representation learning by geometric structure pretraining. *arXiv preprint arXiv:2203.06125*, 2022.

---

## APPENDIX

### A ALL-ATOM DECODING

Given a latent representation at the residue-level,  $(\mathbf{X}, \mathbf{V}^{0:l_{\max}})_i$ , we take  $\mathbf{X}_i$  directly as  $\hat{\mathbf{X}}_i^\alpha$  to obtain the  $\mathbf{C}_\alpha$  position, and transform hidden scalar representations  $\mathbf{V}_i^{l=0}$  into categorical logits over  $\mathcal{R}$  to decode  $\hat{\mathbf{R}}_i$ . We then transform  $\mathbf{V}_i^{l>0}$  to obtain the relative position vectors  $\hat{\mathbf{X}}_i^*$ . The orderable atoms are obtained from  $\mathbf{V}^{l=1}$  while the unorderable pairs are obtained from  $(\mathbf{V}^{l=1}, \mathbf{V}^{l=2})$ . To generate an unorderable pair, we treat  $\mathbf{V}^{l=1}$  as the center position of the symmetric atoms – that is, a "mean vector". We then compute the square root of  $\mathbf{V}^{l=2}$  to establish the relative difference between the two vectors in the unorderable pair. This method proves effective because the sign of the square root is inherently ambiguous. Both positive and negative square root values yield the same  $\mathbf{V}^{l=2}$ , aligning perfectly with our requirement for the vectors to be unorderable.

### B DETAILS ON SELF-INTERACTION

The objective of our Self-Interaction module is to function exclusively based on  $\mathbf{V}^{0:l_{\max}}$ , while concurrently mixing irreducible representations across various  $l$  values. To accomplish this, we calculate the tensor product of the representation with itself; this operation is termed the "tensor square" and is symbolized by  $(\mathbf{V}^{0:l_{\max}})^{\otimes 2}$ . As the channel dimensions expand, the computational complexity tied to the tensor square increases quadratically. In the case of latent diffusion models, we employ the tensor square in its original, unmodified form, accepting the computational cost as a trade-off for maintaining full expressivity. Contrastingly, for autoencoder models, we reduce the computational load by dividing the representation into smaller, independent segments along the channel dimension prior to executing the tensor square. The segmented results are subsequently concatenated to generate the updated representation  $\mathbf{V}^{0:l_{\max}}$ .

### C TRANSPOSE SEQUENCE CONVOLUTION

Given a single, coarse anchor and representation  $\{\mathbf{P}, \mathbf{V}^l\}$ , we first map  $\{\mathbf{V}^l\}$  into  $K$  new representations linearly, reshaping it appropriately. We then similarly map  $\mathbf{V}^{l=1}$  linearly into relative positioning vectors  $[\Delta \mathbf{P}]^K$ , anchoring them in the previous coordinate to obtain  $K$  new coordinates,  $[\mathbf{P}]^K \leftarrow \mathbf{P} + [\Delta \mathbf{P}]^K$ :

---

**Algorithm 6:** Transpose Sequence Convolution

---

**Input:** Kernel Size  $K$  and Stride  $S$ .

**Input:** The Perceptive Field of Varying Size  $P \in \{1, 2\}$  for  $K = 3$  and  $S = 2$

**Input:** Latent Representations  $(\mathbf{P}, \mathbf{V}^{0:l_{\max}})_{1:P}$

**Input:** Relative Indices  $\Delta_{1:P} \in [-\frac{K}{2}, \frac{K}{2}]$

$\mathbf{V}_{1:P}^{0:l_{\max}} \leftarrow \text{Norm} \left( \mathbf{V}_{1:P}^{0:l_{\max}} \right)$  ▷ Normalize  $l$ -Wise

$\mathbf{V}^{0:l_{\max}} \leftarrow \frac{1}{P} \sum_{p=1}^P \text{Linear} \left( \Delta_p, \mathbf{V}_p^{0:l_{\max}} \right)$  ▷ Different Parameters For Each  $\Delta$

$\mathbf{P} \leftarrow \frac{1}{P} \sum_{p=1}^P \left( \mathbf{P}_p + \text{Linear} \left( \Delta_p, \mathbf{V}_p^{l=1} \right) \right)$

**return**  $(\mathbf{P}, \mathbf{V}^{0:l_{\max}})$

---

Windows generated through Transpose Convolutions predict anchoring positions and representations that intersect when mapped back to sequence. We resolve those superpositions by taking the mean anchor and mean representations across intersections.

### D LOSS DETAILS

Our loss function minimizes differences of internal vector maps  $\|V(\mathbf{P}) - V(\hat{\mathbf{P}})\|_1^1$  between predicted and ground positions, where  $V(\mathbf{P})^{i,j} = (\mathbf{P}^i - \mathbf{P}^j) \in \mathbb{R}^{N \times N \times 3}$ . Our output algorithm for decoding atoms produces arbitrary symmetry breaks (Appendix A) for permutation invariances of particular

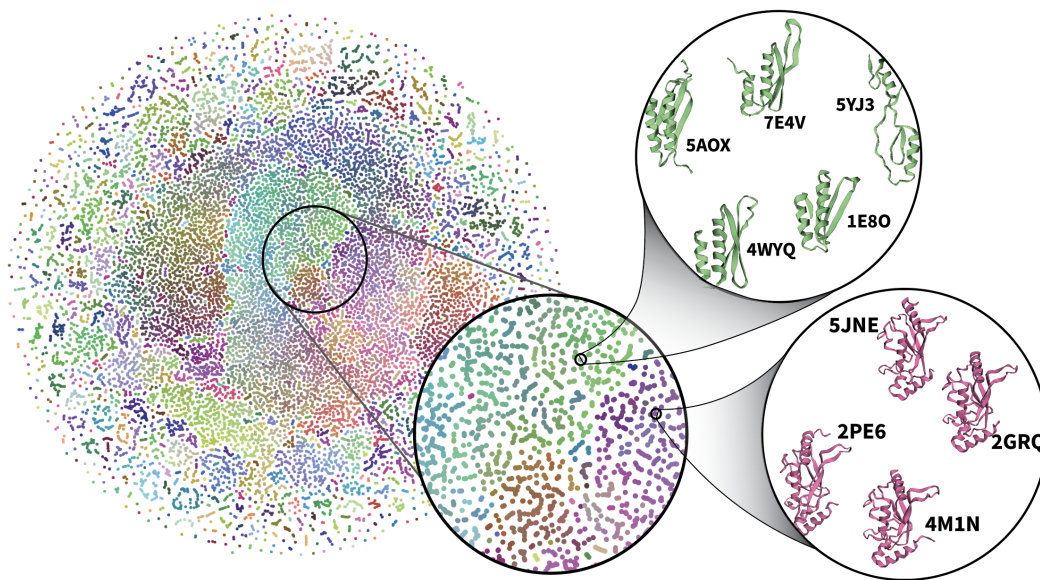


Figure 6: **Latent Space Analysis:** we qualitatively examine the unsupervised clustering capabilities of our representations through t-SNE.

side-chain atoms. Because of that, the vector map loss is not directly applicable to the output of our model. Instead, we first compare vector maps internal to individual residues. We consider the alternative permutation of ground truth positions, and pick the solution which minimizes the vector map loss. We then flip ground truth for the rest to apply the loss across residues in all-atom settings. A similar approach to tackling side-chain symmetries is described by [Jumper et al. (2021)].

## E VISUALIZATION OF LATENT SPACE

To visualize the learned latent space of Ophiuchus, we forward 50k samples from the training set through a large 485-length model (Figure 6). We collect the scalar component of bottleneck representations, and use t-SNE to produce 2D points for coordinates. We similarly produce 3D points and use those for coloring. The result is visualized in Figure 6. Visual inspection of neighboring points reveals unsupervised clustering of similar folds and sequences.

## F MORE ON ABLATION

In addition to all-atom ablation found in Table 1 we conducted a similar ablation study on models trained on backbone only atoms as shown in Table 2. We found that backbone only models performed slightly better on backbone reconstruction. Furthermore, in Fig. 7.a we compare the relative vector loss between ground truth coordinates and the coordinates reconstructed from the auto-encoder with respect to different downsampling factors. We average over different trials and channel rescale factors. As expected, we find that for lower downsampling factors the structure reconstruction accuracy is better. In Fig 7.b we similarly plot the residue recovery accuracy with respect to different downsampling factors. Again, we find the expected result, the residue recovery is better for lower downsampling factors. Notably, the relative change in structure recovery accuracy with respect to different downsampling factors is much lower compared to the relative change in residue recovery accuracy for different downsampling factors. This suggest our model was able to learn much more efficiently a compressed prior for structure as compared to sequence, which coincides with the common knowledge that sequence has high redundancy in biological proteins. In Fig. 7.c we compare the structure reconstruction accuracy across different channel rescaling factors. Interestingly we find that for larger rescaling factors the structure reconstruction accuracy is slightly lower. However, since we trained only for 10 epochs, it is likely that due to the larger number of model

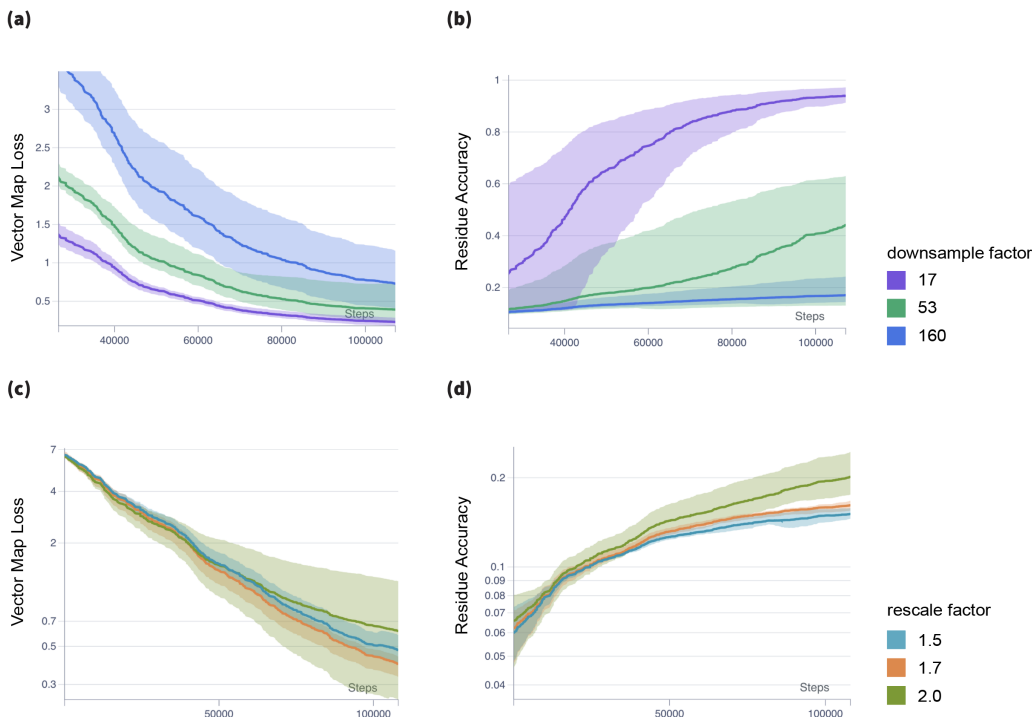


Figure 7: **Ablation Training Curves.** We plot metrics across 10 training epochs for our ablated models from Table 1. **(a-b)** compares models across downsampling factors and highlights the trade-off between downsampling and reconstruction. **(c-d)** compares different rescaling factors for fixed downsampling at 160.

parameters when employing a larger rescaling factor it would take somewhat longer to achieve similar results. Finally, in Fig. 7.d we compare the residue recovery accuracy across different rescaling factors. We see that for higher rescaling factors we get a higher residue recovery rate. This suggests that sequence recovery is highly dependant on the number of model parameters and is not easily capturable by efficient structural models.

Table 2: Recovery rates from bottleneck representations - Backbone only

Factor	Channels/Layer	# Params [1e6]	$C\alpha$ -RMSD ( $\text{\AA}$ )	GDT-TS	GDT-HA
17	[16, 24, 36]	0.34	$0.81 \pm 0.31$	$96 \pm 3$	$81 \pm 5$
17	[16, 27, 45]	0.38	$0.99 \pm 0.45$	$95 \pm 3$	$81 \pm 6$
17	[16, 32, 64]	0.49	$1.03 \pm 0.42$	$92 \pm 4$	$74 \pm 6$
53	[16, 24, 36, 54]	0.49	$0.99 \pm 0.38$	$92 \pm 5$	$74 \pm 8$
53	[16, 27, 45, 76]	0.67	$1.08 \pm 0.40$	$91 \pm 6$	$71 \pm 8$
53	[16, 32, 64, 128]	1.26	$1.02 \pm 0.64$	$92 \pm 9$	$75 \pm 11$
160	[16, 24, 36, 54, 81]	0.77	$1.33 \pm 0.42$	$84 \pm 7$	$63 \pm 8$
160	[16, 27, 45, 76, 129]	1.34	$1.11 \pm 0.29$	$89 \pm 4$	$69 \pm 7$
160	[16, 32, 64, 128, 256]	3.77	$0.90 \pm 0.44$	$94 \pm 7$	$77 \pm 9$

## G ADDITIONAL CONFORMATIONAL INTERPOLATION

We provide an additional example from PDBFlex in Fig. 8.

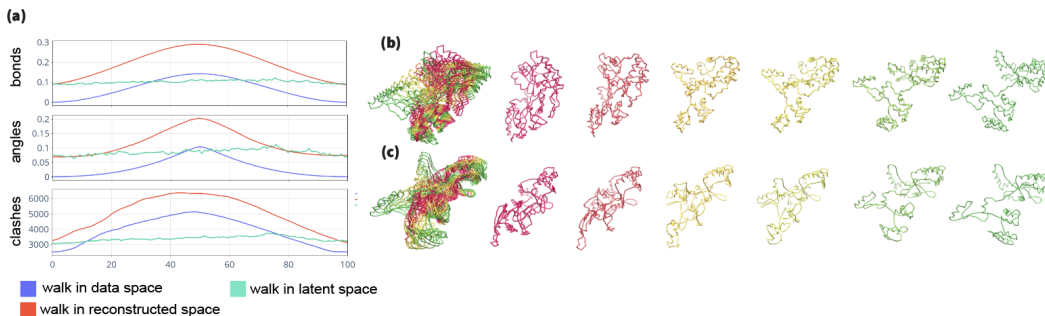


Figure 8: **(a)** Comparison of chemical validity metrics across interpolated structures of Maltose-binding periplasmic protein (PDB ID: 4JKM and PDB 6LF3). We plot results for interpolations on the original data space, on the latent space, and on the autoencoder-reconstructed data space. **(b)** Direct linear interpolation of coordinates. **(c)** Decoded linear latent interpolation between the same encoded states as in (b).

## H DIFFUSION DETAILS

To train an autoencoder for latent diffusion over the miniprotein library, we instantiate an Ophiuchus model with stride  $S = 3$  and kernel size  $K = 5$ . The model progressively coarsens sequences across lengths [63, 31, 15, 7, 3, 1] while producing representations of dimensionalities [12, 18, 27, 40, 60, 90].

We regularize the learned latent space so that representations are amenable to the range scales of diffusion. Let  $\mathbf{V}_i^l$  denote the  $i$ -th channel of a vector representation  $\mathbf{V}^l$ . We regularize the autoencoder latent space by optimizing radial and angular components of our vectors:

$$\mathcal{L}_{\text{reg}} = \sum_i \text{ReLU}(1 - \|\mathbf{V}_i^l\|_1) + \sum_i \sum_{i \neq j} (\mathbf{V}_i^l \cdot \mathbf{V}_j^l)$$

The first term penalizes vector magnitudes larger than one, and the second term induces vectors to spread angularly. We find these regularizations to significantly help training of the denoising diffusion model. The diffusion model uses Self-Interactions with full tensor product [B].

To compute the scTM scores, we recover 8 sequences using ProteinMPNN for all sampled backbones from our diffusion model. We used a sampling temperature of 0.1 for ProteinMPNN. Unlike the original work, where the sequences were folded using AlphaFold2, we use OmegaFold [Wu et al. (2022)] similar to [Lin & AlQuraishi (2023)]. The predicted structures are aligned to the original sampled backbones and TM-Score is calculated for each alignment. For the all-atom generation we calculated the TM-scores by folding the generated sequence using OmegaFold (Fig. 5.b.)